Chinese Chemical Letters 37 (2026) 110964

Contents lists available at ScienceDirect

Chinese Chemical Letters

journal homepage: www.elsevier.com/locate/cclet

Artificial intelligence-driven development of natural multi-target derivatives with BuChE inhibitory activity for treating Alzheimer's disease

Qiyao Zhang[a,b,1], Yuting Li[a,c,1], Qishun Jin[a,1], Zhengwei Liu[a,d,1], Hongsong Chen[e], Jingqi Huang[a], Taoyi Liu[a], Xiaojuan Liu[a], Zhenghuai Tan[f], Shuheng Huang[a,*], Wu Dong[e,*], Zhipei Sang[a,*]

[a] Key Laboratory of Tropical Biological Resources of Ministry of Education and One Health Institute, School of Pharmaceutical Sciences, Hainan University, Haikou 570228, China
[b] School of Food Science and Engineering, Hainan University, Haikou 570228, China
[c] School of Life and Health Sciences, Hainan University, Haikou 570228, China
[d] College of Chemistry and Pharmaceutical Engineering, Nanyang Normal University, Nanyang 473061, China
[e] College of Animal Science and Technology, Inner Mongolia Minzu University, Tongliao 028000, China
[f] Institute of Traditional Chinese Medicine Pharmacology and Toxicology, Sichuan Academy of Chinese Medicine Sciences, Chengdu 610041, China

ARTICLE INFO

Article history:
Received 9 December 2024
Revised 14 February 2025
Accepted 17 February 2025
Available online 17 February 2025

Keywords:
Alzheimer's disease
AI-driven
Multifunctional agents
BuChE inhibitor
In vivo study

ABSTRACT

Alzheimer's disease (AD) is a common neurodegenerative disorder among the elderly population. There are currently no effective therapeutic drugs available, the multi-target-directed ligands (MTDLs) strategy has been considered as the promising approach. Given the structural diversity of natural products, Rivastigmine's pharmacophore was integrated with diverse natural product scaffolds to construct a combinatorial compound library. This library was subsequently screened and optimized to identify a novel butyrylcholinesterase (BuChE) inhibitor, compound **3c**. The results showed that compound **3c** exhibited favorable BuChE inhibitory activity (half-maximal inhibitory concentration (IC_{50}) = 0.43 μmol/L), potential anti-inflammatory potency, good Aβ_{1-42} aggregation inhibitory capacity and remarkable neuroprotective effects. The *in vivo* study exhibited that **3c** significantly ameliorated $AlCl_3$-induced zebrafish AD model and scopolamine-induced memory impairment. Collectively, compound **3c** was the artificial intelligence (AI)-driven promising multifunctional agent with BuChE inhibition for the treatment of AD.

© 2025 Published by Elsevier B.V. on behalf of Chinese Chemical Society and Institute of Materia Medica, Chinese Academy of Medical Sciences.

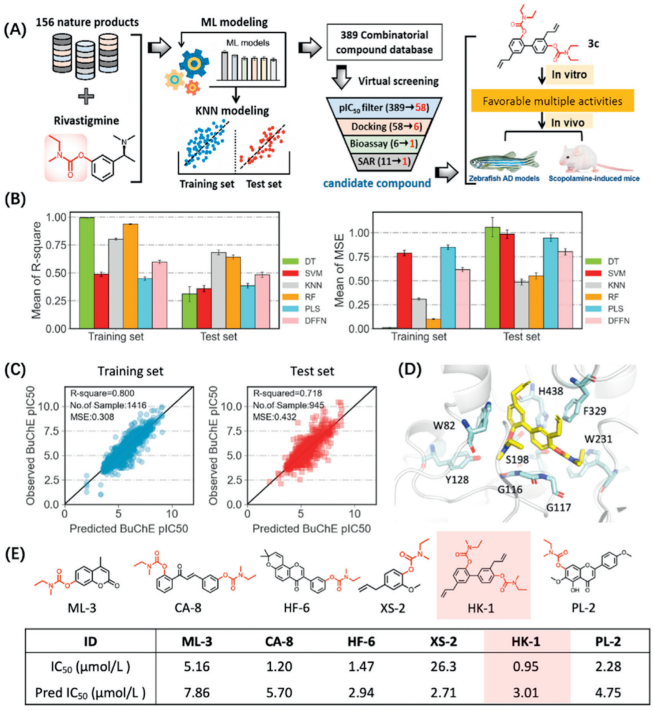
Alzheimer's disease (AD) is a progressive neurodegenerative disorder characterized by deteriorating memory, declining language skills, and a range of cognitive impairments in older adults [1]. As of now, over 55 million individuals worldwide are diagnosed with AD, a figure projected to rise to 78 million by 2030 [2]. The disease exerts substantial social and economic impacts. Currently, there are no effective therapeutic options available for its treatment.

Despite considerable research efforts, the precise etiology of AD remains unclear. Pathological alterations observed in the brains of AD patients include decreased levels of acetylcholine (ACh), the accumulation of amyloid-β (Aβ) deposits, heightened oxidative stress, hyperphosphorylated tau neurofibrillary tangles, dysregulation of biometal ions, and inflammation [2,3]. The complexity inherent in the etiology of AD has prompted researchers to investigate multi-target-directed ligands (MTDLs) as a promising therapeutic strategy. MTDLs are designed to interact simultaneously with multiple disease-related targets, aiming to produce a synergistic effect that enhances clinical outcomes [4–6].

The classical "cholinergic hypothesis" posits that the neurotransmitter ACh is critical for nerve cell function related to learning and memory. Abnormally low levels of ACh in the hippocampus and neocortex are directly linked to cognitive decline in AD [7]. Acetylcholinesterase (AChE) and butyrylcholinesterase (BuChE) are two key enzymes in this context, with BuChE typically acting as a backup to AChE. In AD patients, AChE levels can decline by up to 90%, while BuChE levels may increase to around 165% of normal [8,9]. This shift suggests that BuChE compensates for the diminished AChE activity in ACh hydrolysis. Inhibition of BuChE has

* Corresponding authors.
E-mail addresses: shhuang@hainanu.edu.cn (S. Huang), dongwu@imun.edu.cn (W. Dong), sangzhipei@hainanu.edu.cn (Z. Sang).
[1] These authors contributed equally to this work.

https://doi.org/10.1016/j.cclet.2025.110964
1001-8417/© 2025 Published by Elsevier B.V. on behalf of Chinese Chemical Society and Institute of Materia Medica, Chinese Academy of Medical Sciences.



ID	ML-3	CA-8	HF-6	XS-2	HK-1	PL-2
IC_{50} (μmol/L)	5.16	1.20	1.47	26.3	0.95	2.28
Pred IC_{50} (μmol/L)	7.86	5.70	2.94	2.71	3.01	4.75

Fig. 1. Schematic illustration of *de novo* design and development of hBuChE inhibitors for ameliorating AD. (A) Entire workflow for developing efficacious hBuChE inhibitors. (B) The performance of the 5 ML models and the DFNN model on the training and test dataset. Default parameters were used for the ML models if not specified. Data are presented as mean ± standard deviation (SD) ($n = 100$). (C) Observed *vs.* predicted pIC_{50} of the 1416 training and 945 test samples. pIC_{50} is $-\log_{10}(IC_{50})$. (D) The optimal binding mode of **HK-1**. (E) Schematic diagram and the bioassay results of 6 representative compounds.

shown promise in reducing the aggregation of fibrillogenic $A\beta_{1-42}$ peptides, and studies utilizing BuChE knockout models have revealed no significant physiological deficits, indicating its potential as a therapeutic target in advanced AD [10–12]. Many selective BuChE inhibitors have been developed and successfully applied for treating AD [8,13]. Therefore, developing MTDLs with BuChE inhibition represents a promising approach for treating AD.

Natural products are extensively researched for their potential in developing anti-AD drugs, owing to their significant advantages, such as structural diversity and inherent multifunctional biological activities [14–17]. For instance, natural flavonoid compounds are investigated for their antioxidant, anti-inflammatory, and neuroprotective properties; however, their clinical application is hindered by low bioavailability and poor permeability across the blood-brain barrier. Rivastigmine, a pseudo-irreversible, carbamate-type, brain-selective dual inhibitor of AChE and BuChE, has been approved by the Food and Drug Administration (FDA) for the treatment of AD [18]. The carbamate moiety of rivastigmine is recognized as the pharmacophore responsible for its cholinesterase inhibitory activity [19–21]. By integrating the pharmacophore of rivastigmine with the core scaffolds derived from natural products, it is anticipated that multi-target BuChE inhibitors can be developed as promising candidates for AD therapy.

In this study, we propose a strategy that integrates combinatorial compound design, machine learning (ML)-based virtual screening, and structure-activity relationship (SAR) studies for the *de novo* design of BuChE inhibitors and the assessment of their anti-AD activity [22–24]. As shown in Fig. 1A, the overall research framework consists of the following steps: (i) designing a combinatorial compound library based on natural products and rivastigmine; (ii) constructing ML-based activity prediction models; (iii) identifying hit compounds through multistep virtual screening; and (iv) evaluating anti-AD drug efficacy *in vitro* and *in vivo* studies. Employing this approach, we identified a novel BuChE inhibitor, designated as compound **3c** (half maximal inhibitory concentration (IC_{50}) = 0.43 μmol/L). Docking simulations and molecular dynamics studies provided a rational basis for its enhanced activity. The significant efficacy of compound **3c** warranted comprehensive investigations into its reversible inhibition, neuroprotective effects, drug-likeness, pharmacokinetics, and safety profile. *In vivo* studies were conducted using AD zebrafish models and scopolamine-induced mice. These findings represent a substantial advancement in the design and development of highly specific and potent BuChE inhibitors, positioning compound **3c** as a promising candidate for the treatment of AD.

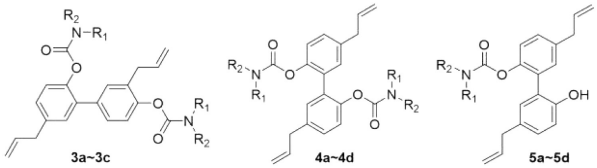
Herein, 156 natural products were selected as core scaffolds. Considering the carbamate moiety as a critical pharmacophore in Rivastigmine, carbamate modifications were introduced at the *ortho*, *meta*, and *para* positions of the selected scaffolds. This strategy led to the construction of a library containing 389 fragment-based combinatorial compounds. To develop an accurate ML predictor for BuChE inhibitory activities, we created a database of 2689 compounds with varying inhibition levels, sourced from the literature. After removing duplicates and ambiguous data, 2361 compounds remained. We then applied five ML models-support vector machine (SVM), logistic regression (LR), k-nearest neighbor (KNN), random forest (RF), partial least squares (PLS), and a deep feed-forward neural network (DFNN). Based on prediction accuracy and balanced test set performance (Figs. 1B and C), we selected KNN as the optimal model. This choice was supported by robust statistical metrics: R^2 of 0.800 and mean squared error (MSE) of 0.308 for the training set, and R^2 of 0.718 with MSE of 0.432 for the test set, with a relative error under 25 %, demonstrating high reliability.

We first used the optimal KNN model to predict the activity of 389 combinatorial compounds, resulting in the identification of 58 compounds with predicted pIC_{50} values greater than 5, indicating micromolar-level activity. These 58 compounds were then prioritized for further analysis through molecular docking and virtual screening, which led to the selection of 6 promising candidates for chemical synthesis and bioactivity testing (Figs. 1D and E). The optimized compounds with their detailed properties were summarized in Fig. 1E. The results demonstrated that the ML model provided accurate predictions of compound activity, reflected by the consistent correlation between predicted and observed pIC_{50} values. Among these, compound **HK-1** stood out with its submicromolar inhibitory activity, making it a top candidate for further optimization as a lead compound.

To develop more effective BuChE inhibitors, we conducted structural optimization and SAR studies based on the lead compound **HK-1** (Fig. S1 in Supporting information). The synthetic routes for the novel target derivatives were illustrated in Schemes S1–S3 (Supporting information). In brief, as shown in Schemes S1 and S2, commercially available starting materials, honokiol (**1a**) or magnolol (**1b**) (2.0 mmol), were treated with excess *N*,*N*-disubstituted carbamoyl chlorides (**2a**–**2d**) (5.0 mmol), including *N*-ethyl-*N*-methylcarbamoyl chloride (**2a**), dimethylcarbamoyl chloride (**2b**), diethylcarbamoyl chloride (**2c**), and diisopropylcarbamoyl chloride (**2d**), in the presence of K_2CO_3 in CH_3CN at 60–65 °C, yielding target compounds **3a**–**3c** and **4a**–**4d**, respectively. Subsequently, as depicted in Scheme S3, magnolol (**1a**) (2.0 mmol) was reacted with excess *N*,*N*-disubstituted carbamoyl chlorides (**2a**–**2d**) (3.0 mmol), respectively, under the same reaction conditions to obtain target compounds **5a**–**5d.**

In order to evaluate the AChE/BuChE inhibitory activity of target derivatives, the modified Ellman's method was applied using *Electrophorus electricus* AChE (*ee*AChE) and equine serum BuChE (*eq*BuChE) [25]. As listed in Table 1, when changing *N*-

Table 1
Inhibition of AChE/BuChE by the synthesized compounds **3**–**5**, and the positive compounds.



Compound	NR_1R_2	IC_{50} (μmol/L)[a]		SI[b]	Inhibition of self-induced Aβ_{1-42} aggregation (%) [d]
		*ee*AChE	*eq*BuChE		
3a		11.2 ± 0.29	0.95 ± 0.08	11.8	NT [e]
3b		10.7 ± 0.63	1.2 ± 0.51	8.9	NT [e]
3c		13.1 ± 0.29	0.43 ± 0.03	30.5	63.4 ± 2.37
4a		12.5 ± 0.61	10.3 % ± 0.52 %[c]	–	NT [e]
4b		15.4 ± 0.87	12.0 % ± 0.61 %[c]	–	NT [e]
4c		16.6 ± 0.95	8.3 % ± 0.14 %[c]	–	NT [e]
4d		6.8 ± 0.34	6.7 % ± 0.22 %[c]	–	NT [e]
5a		8.9 ± 0.21	13.8 ± 0.55	0.6	NT [e]
5b		17.9 ± 0.88	15.7 % ± 0.86 %[c]	–	NT [e]
5c		14.3 ± 0.82	18.7 % ± 0.69 %[c]	–	NT [e]
5d		16.6 ± 0.95	10.7 % ± 0.33 %[c]	–	NT [e]
Rivastigmine		11.6 ± 0.93	5.3 ± 0.27	2.2	NT [e]
Donepezil		0.021 ± 0.002	6.8 ± 0.03	0.003	NT [e]
Curcumin					47.3 ± 3.18

[a] The IC_{50} values represent the concentration of the inhibitor required to reduce enzyme activity by 50 %. These values are reported as the mean of three independent experiments.
[b] SI = selectivity index = IC_{50} (AChE)/IC_{50} (BuChE).
[c] The inhibition percentage of *eq*BuChE at a concentration of 12.5 μmol/L was determined.
[d] The inhibition of self-induced Aβ_{1-42} aggregation was evaluated at 25 μmol/L.
[e] NT indicates that no tests were performed.

ethyl-*N*-methylcarbamate of **3a** (**HK-1**) with dimethylcarbamate to get compound **3b**, the BuChE inhibition slightly decreased to 1.2 μmol/L, while replacing *N*-ethyl-*N*-methylcarbamate of **3a** with diethylcarbamate to afford compound **3c**, the BuChE inhibitory potency significantly improved to 0.43 μmol/L. Moreover, when replacing the honokiol skeleton of **3a** (**HK-1**) with magnolol skeleton to obtain compound **4a**, demonstrating weak BuChE inhibition (10.3 % at 12.5 μmol/L) and moderate AChE inhibition (IC_{50} = 12.5 μmol/L). And the SAR exhibited that replacing *N*-ethyl-*N*-methylcarbamate of **4a** with dimethylcarbamate, diethylcarbamate and diisopropylcarbamoyl to get derivatives **4c**–**4d**, respectively, indicating weak BuChE inhibition and AChE inhibition (except **4d**, IC_{50} = 6.8 μmol/L). Further, replacing bissubstituted carbamates of **4a**–**4d** with monosubstituted carbamates to afford derivatives **5a**–**5d**, respectively. The data showed that compounds **5a**–**5d** indicating moderate to good *ee*AChE inhibitory activity with IC_{50} values from 8.9 μmol/L to 17.9 μmol/L, and weak *eq*BuChE inhibitory potency. Among of these derivatives, compound **5a** with monosubstituted *N*-ethyl-*N*-methylcarbamate derivative showed moderate *ee*AChE inhibition (IC_{50} = 8.9 μmol/L) and weak *eq*BuChE inhibition (IC_{50} = 13.8 μmol/L), which did not reach up to our expectations. The results suggested that magnolol was not ideal skeleton to develop BuChE inhibitor. As a whole, through multiple rounds of compound efforts, we finally obtained the most promising selective *eq*BuChE inhibitor **3c** (IC_{50} = 0.43 μmol/L), deserving to further investigate.

The active site of BuChE is a narrow hydrophobic cavity, with Ser198 and His438 serving as the catalytic active sites, while Trp231 and Leu286 form the acyl binding pocket (Fig. 2A). Herein, to accurately evaluate the binding free energy of hit compound **3c** with BuChE, we performed binding free energy studies [26,27]. The binding stability of compound **3c** with BuChE was evaluated using GROMACS 2022.5. During the 50 ns molecular dynamics (MD) simulation, the system remained stable (Fig. S2 in Supporting information). The root mean square deviation (RMSD) of the complex and protein fluctuations remained below 2 Å during the last 20 ns, indicating that the binding of **3c** with BuChE had stabilized (Fig. 2B and Fig. S3 in Supporting information). The lowest energy conformation revealed that compound **3c** snugly fitted into a hydrophobic pocket formed by residues Trp82, Thr120, Glu197,

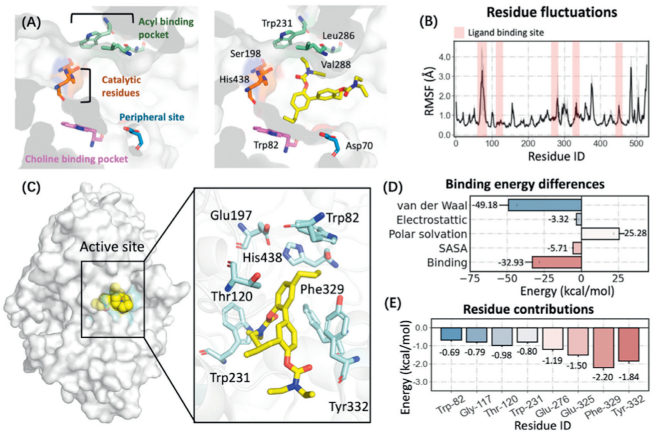


Fig. 2. The binding mode of hit compound **3c** in BuChE active pocket. (A) Key residues of BuChE (PDB code: 4TPK). (B) The root mean square fluctuation (RMSF) of protein during 50 ns MD simulations. Error bars represent standard deviation of three experiments. (C) The lowest energy binding mode of **3c**-BuChE complex. The compound is shown in yellow stick mode. Key residues of BuChE are depicted in cyan stick mode. (D) Total binding free energy and its component. SASA: solvent accessible surface area energy. (E) Residue contribution of hot residues for receptor-ligand combination.

Trp231, Phe329, Tyr332, and His438 (Fig. 2C). It was worth noting that diethylcarbamate was embedded in a narrow hydrophobic cavity formed by Trp231 and Val228, where it formed van der Waals interactions. The total binding free energy was calculated as −32.93 kcal/mol, with van der Waals interactions contributing significantly to the ligand-receptor binding (−49.18 kcal/mol) (Fig. 2D). Key residues such as Phe329 (−2.20 kcal/mol), Tyr332 (−1.84 kcal/mol), and Glu325 (−1.50 kcal/mol) played crucial roles in the interaction between **3c** and human BuChE (hBuChE), emphasizing their importance in stabilizing the ligand binding (Fig. 2E).

To assess the reversible inhibition of BuChE by compound **3c**, we conducted a time-course evaluation of BuChE activity recovery following a dilution protocol [28]. As depicted in Fig. 3A, treatment with $0.1 \times IC_{50}$ of donepezil resulted in a significant restoration of BuChE activity, increasing from 47.8 % to 77.8 % over 240 min, indicating its characteristic reversible inhibition. In contrast, BuChE activity in the presence of $0.1 \times IC_{50}$ of rivastigmine remained relatively stable throughout the 240-min observation period, with no significant recovery. Notably, **3c** exhibited a profile similar to that of rivastigmine, suggesting that it might act as a *pseudo*-irreversible inhibitor of BuChE.

Compound **3c** was selected to evaluate its anti-inflammatory activity by assessing the production of nitric oxide (NO) and interleukin-6 (IL-6) in lipopolysaccharide (LPS)-induced BV-2 microglial cells [29]. As shown in Fig. 3B, compound **3c** exhibited a favorable safety profile with minimal cytotoxicity at concentrations below 10 μmol/L. Moreover, as illustrated in Figs. 3C and D, compound **3c** significantly reduced the production of NO and the secretion of IL-6 in a dose-dependent manner. Collectively, these findings suggested that compound **3c** had potential as an anti-inflammatory agent. The effects of **3c** on self-induced Aβ_{1-42} aggregation were evaluated using the thioflavin T (ThT) fluorescence assay, with curcumin serving as a positive control [30]. As summarized in Table 1, at a concentration of 25 μmol/L, compound **3c** exhibited a significant inhibitory effect on self-induced Aβ_{1-42} aggregation, achieving an inhibition rate of 63.4 %, surpassing that of curcumin, which was 47.3 %.

The neuroprotective effects of compound **3c** were evaluated in Glu-/Aβ_{25-35}-induced HT22 cell injury using the cell counting kit-8 (CCK-8) assay, with rivastigmine included as a positive control [30]. As shown in Fig. 3E, **3c** displayed minimal cytotoxicity in HT22 cells at concentrations below 40 μmol/L. Fig. 3F illustrated that exposure to 500 μmol/L L-glutamic acid significantly reduced cell viability to 50.0 % ($P < 0.01$). In contrast, treatment with various concentrations of compound **3c** and rivastigmine (1, 2, 4, 8, and 16 μmol/L) resulted in a significant dose-dependent increase in cell viability, indicating that the neuroprotective potential of **3c** was markedly superior to that of rivastigmine. Furthermore, as demonstrated in Fig. 3G, compound **3c** provided significant neuroprotection against Aβ_{25-35}-induced injury in HT22 cells in a similar dose-dependent manner compared to rivastigmine. Collectively, these findings suggested that compound **3c** offered substantial neuroprotective effects against Glu- and Aβ_{25-35}-induced cellular injury, underscoring its potential therapeutic relevance in neurodegenerative disorders.

The permeability of the blood-brain barrier (BBB) is a critical factor in the development of effective therapeutic agents for AD [31]. In this context, compound **3c** was evaluated for its BBB permeability using a parallel artificial membrane permeation assay for the BBB (PAMPA-BBB). Initial validation of the PAMPA-BBB approach involved 11 well-characterized drugs with known

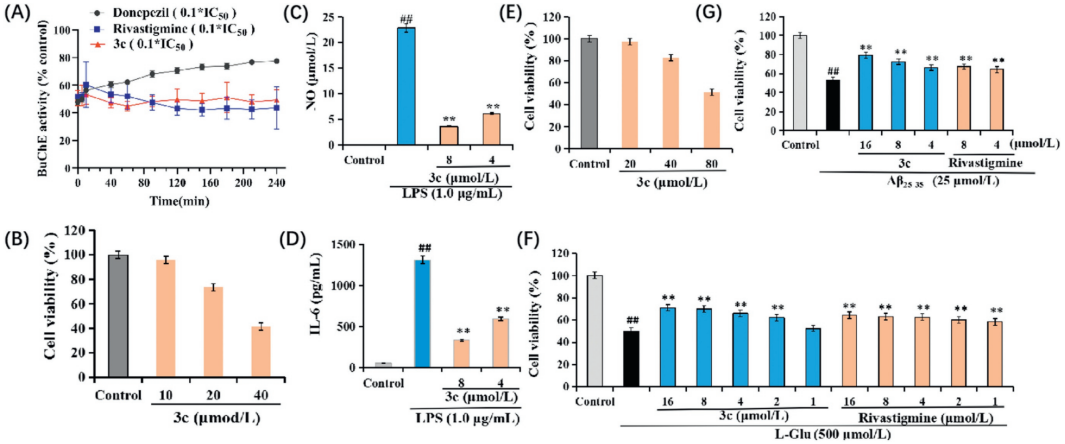


Fig. 3. (A) The recovery of BuChE inhibitors (donepezil, rivastigmine and **3c**) inhibition after dilution with time monitoring. (B) The cell viability of compound **3c** on BV-2 cells was assessed using the CCK-8 assay. (C) Effects of compound **3c** on NO release in LPS-stimulated BV-2 cells. (D) Effects of compound **3c** on IL-6 production in LPS-stimulated BV-2 cells. (E) Cell viability (%) of compound **3c** in HT22 cells. (F) Neuroprotective effects of compounds **3c** and rivastigmine on Glu-induced injury in HT22 cells. (G) Neuroprotective effects of compounds **3c** and rivastigmine on Aβ_{25-35}-induced injury in HT22 cells. Data are presented as mean ± SD from three independent experiments. $^{\#\#}P < 0.01$ *vs.* control group; $^{**}P < 0.01$ *vs.* Glu/Aβ_{25-35}-induced group.

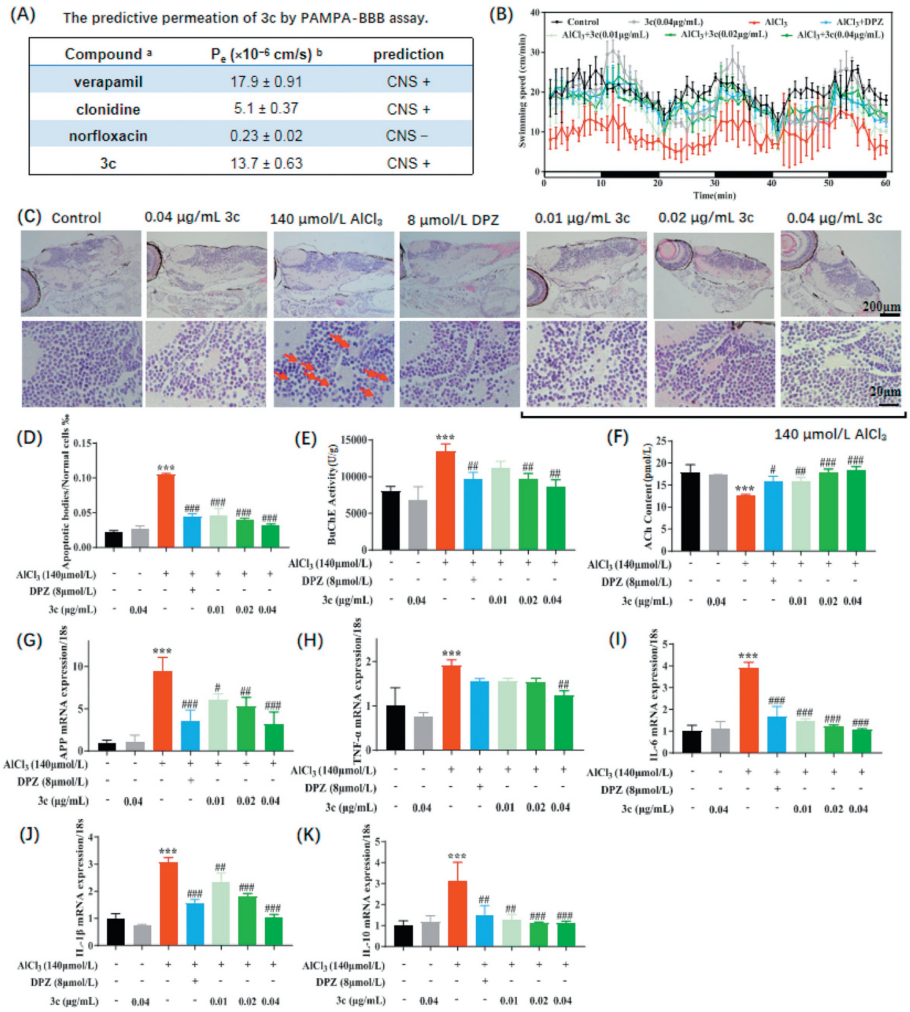


Fig. 4. Effects of **3c** in the $AlCl_3$-induced zebrafish model. (A) The predictive permeation of **3c** by PAMPA-BBB assay. [a] Compound **3c** was dissolved in DMSO at a concentration of 5 mg/mL and subsequently diluted with PBS/EtOH (70:30) to achieve a final concentration of 100 μg/mL. [b] Values are expressed as the mean ± SD from three independent experiments. CNS, central nervous system. (B) Behavioral changes in the zebrafish larvae per minute. DPZ, donepezil. (C) The apoptotic body/normal cells in the various zebrafish models were statistically analyzed after HE staining. Scale bar: top (200 μm), bottom (20 μm). (D) Apoptotic body changes in the brain of zebrafish were performed using HE staining. (E) BuChE activity changes in various zebrafish group. (F) ACh level changes in various zebrafish group. (G) APP mRNA expression changes in various zebrafish group. (H) TNF-α mRNA expression changes in various zebrafish group. (I) IL-6 mRNA expression changes in various zebrafish group. (J) IL-1β mRNA expression changes in various zebrafish group. (K) IL-10 mRNA expression changes in various zebrafish group. (D-K) Data are presented as mean ± SD ($n = 3$). $^{***}P < 0.001$ *vs.* control group. $^{\#}P < 0.05$, $^{\#\#}P < 0.01$, $^{\#\#\#}P < 0.001$ *vs.* $AlCl_3$-induced zebrafish model.

BBB permeability profiles, as reported in our previous studies [32]. The following permeability classifications were established: $P_e < 1.61 \times 10^{-6}$ cm/s indicated weak BBB permeation; $1.61 < P_e < 3.44 \times 10^{-6}$ cm/s indicated uncertain BBB permeation; and $P_e > 3.44 \times 10^{-6}$ cm/s signified high BBB permeability. As outlined in Fig. 4A, the calculated P_e value for compound **3c** was 13.7×10^{-6} cm/s, indicating that compound **3c** had a high capacity to cross the BBB *in vitro*, thereby supporting its potential as a therapeutic candidate for AD.

The exceptional biological characteristics of zebrafish provide a valuable complement to traditional drug development models [33]. Initially, we assessed the safety profile of compound **3c** using six different concentrations (10.0, 5.0, 2.5, and 1.25 μg/mL) in a zebrafish model (Fig. S4 in Supporting information). Notably, no mortality was observed at 1.25 μg/mL over a 48-min exposure period. Following this, we conducted a more detailed evaluation of developmental toxicity by examining pericardial edema relative to body length and the swim bladder area at two concentrations (1.25 and 0.625 μg/mL). The results indicated a significant reduction in both pericardial edema/body length and swim bladder area at the higher concentration of 1.25 μg/mL. Conversely, at 0.625 μg/mL, there were no statistically significant changes observed.

The $AlCl_3$-induced zebrafish AD model is a well-established platform for the rapid screening of potential anti-AD agents [30,34]. Based on the previously determined maximum tolerable concentration (MTC) of 0.625 μg/mL for compound **3c**, we subsequently selected three lower concentrations (0.01, 0.02, and 0.04 μg/mL) for further evaluation following preliminary screening. To assess the therapeutic effects of these treatments, a series of behavioral tests were conducted under alternating light and dark conditions over a 60-min period (Fig. 4B). The experimental design included seven groups: control group, **3c** treatment group, $AlCl_3$-induced model group, $AlCl_3$ + donepezil group, and $AlCl_3$ + **3c** treatment groups at concentrations of 0.01, 0.02, and 0.04 μg/mL. As shown in Figs. S5A–C (Supporting information), zebrafish exposed to $AlCl_3$ demonstrated a statistically significant reduction in swimming distance compared to the control group under both light and dark conditions. In contrast, treatment with donepezil and compound **3c** at concentrations of 0.01, 0.02, and 0.04 μg/mL resulted in a marked increase in swimming distance, indicating an

ameliorative effect on locomotor activity. Furthermore, the cumulative analysis of total swimming distance over the 60-min period (Fig. S5C in Supporting information) revealed that both donepezil and compound **3c** at all tested concentrations significantly enhanced the total swimming distance when compared to the $AlCl_3$-induced zebrafish model group. These findings suggest that compound **3c** exhibits potential anti-AD activity that warrants further investigation.

Furthermore, swimming speed significantly decreased in the $AlCl_3$-induced zebrafish AD group compared with the control group during light conditions, respectively (Fig. S5D in Supporting information). Following treatment with donepezil and **3c** (0.01, 0.02, and 0.04 μg/mL), the swimming speed remarkably improved compared with the model group. And this trend was also observed under dark conditions (Fig. S5E in Supporting information**)**. Additionally, the total swimming speed over the 60-min period demonstrated that both donepezil and **3c** (0.01, 0.02 and 0.04 μg/mL) significantly increased swimming speed compared with the $AlCl_3$-induced zebrafish AD group (Fig. S5F in Supporting information). During the transition from light to dark (Fig. S5G in Supporting information), donepezil and **3c** (0.04 μg/mL) significantly enhanced reaction capacity compared to the $AlCl_3$-induced zebrafish AD group. Further, the switch from dark to light revealed that both donepezil and **3c** (0.01, 0.02 and 0.04 μg/mL) significantly enhanced reaction capacity compared to the $AlCl_3$-induced zebrafish AD group (Fig. S5H in Supporting information).

Following behavioral assessments, we conducted histopathological analyses using hematoxylin and eosin (HE) staining, as depicted in Figs. 4C and D. The findings indicated that treatment with $AlCl_3$ resulted in a significant increase in the number of apoptotic cells within the zebrafish brains. In contrast, administration of compound **3c** at concentrations of 0.01, 0.02, and 0.04 μg/mL led to a significant reduction in apoptotic cell counts in a dose-dependent manner, yielding results comparable to those observed with donepezil. Furthermore, Figs. 4E and F illustrated that compound **3c** elevated ACh levels by inhibiting BuChE, thereby exerting anti-AD effects. Additionally, compound **3c** was associated with a decrease in the levels of amyloid precursor protein (APP), as shown in Fig. 4G, suggesting a potential mechanism for mitigating amyloidogenesis. Moreover, **3c** demonstrated substantial anti-inflammatory activity, evidenced by the reduction of pro-inflammatory cytokines, including human tumor necrosis factor alpha (TNF-α, Fig. 4H), interleukin-6 (IL-6, Fig. 4I), IL-1β (Fig. 4J), and IL-10 (Fig. 4K). In summary, the cumulative findings from this study indicated that **3c** significantly ameliorated the effects of the $AlCl_3$-induced zebrafish AD model by inhibiting BuChE activity and elevating ACh levels. Additionally, **3c** exhibited remarkable anti-inflammatory properties and reduced APP levels, underscoring its potential as a therapeutic agent in the management of AD.

Compound **3c** was selected to evaluate its effects on memory deficits induced by scopolamine in mice, using the step-down passive avoidance task as the primary assessment method. Animal studies were conducted in accordance with the approved protocol by the Animal Ethics Committee of the Sichuan Academy of Traditional Chinese Medicine (IACUC) (approval number: R-20240721–01). To establish the safety profile of **3c**, Kunming mice (18–22 g) were administered 500 mg kg^{-1} day^{-1} *via* gavage for 14 days. The treatment did not result in any significant changes in movement behavior, mental state, or body weight, indicating a favorable safety profile. Subsequently, the efficacy of **3c** in alleviating scopolamine-induced memory deficits was assessed [25,28]. As shown in Fig. 5, administration of 5.0 mg/kg scopolamine resulted in a significant decrease in step-down latency to 51.7 s in the model group ($P < 0.01$), compared to 239.8 s in the control group. Treatment with 5.0 mg/kg donepezil significantly improved step-down latency, increasing it to 186.0 s ($P < 0.01$) relative to the model group. Furthermore, treatment with compound **3c** at doses of 5.6 and 16.8 mg/kg resulted in step-down latencies of 90.7 and 183.5 s ($P < 0.01$), respectively, demonstrating that **3c** significantly mitigated scopolamine-induced memory impairment.

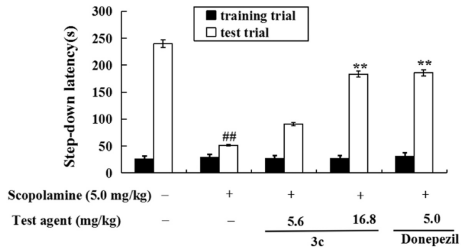


Fig. 5. Effects of **3c** (5.6 and 16.8 mg/kg) and donepezil (5.0 mg/kg) on scopolamine-induced memory impairment were assessed using the step-down passive avoidance assay. Data are presented as mean ± SD ($n = 10$). $^{\#\#}P < 0.01$ *vs.* the control group; $^{**}P < 0.01$ *vs.* the model group.

AD is a chronic, progressive neurodegenerative disorder primarily observed in the elderly population. To date, there are no effective treatments available. The MTDLs strategy is considered one of the most promising approaches for addressing the complex pathogenesis of AD. Natural products have been extensively investigated for their potential anti-AD effects due to their diverse chemical structures and multiple pharmacological activities. However, their clinical applications are often limited by low bioavailability and poor permeability across the BBB. Rivastigmine, an FDA-approved dual cholinesterase inhibitor for the treatment of AD, contains a carbamate moiety that is crucial for its pharmacological activity. To develop natural product-derived multi-target compounds with BuChE inhibitory activity, we constructed a combinatorial compound library based on natural products, ultimately identifying a novel BuChE inhibitor, **HK-1**, as the lead compound through multi-step virtual screening.

Subsequently, **HK-1** underwent several rounds of structural optimization, resulting in candidate compound **3c.** Results demonstrated that compound **3c** exhibited favorable BuChE inhibitory activity ($IC_{50} = 0.43$ μmol/L) and potential anti-inflammatory properties. Furthermore, compound **3c** displayed significant inhibitory capacity against $A\beta_{1-42}$ aggregation and remarkable neuroprotective effects. *In vivo* studies revealed that **3c** significantly ameliorated the effects of $AlCl_3$-induced zebrafish AD model by inhibiting BuChE activity and elevating ACh levels. Additionally, **3c** demonstrated notable anti-inflammatory effects and reduced levels of APP. Importantly, compound **3c** also improved scopolamine-induced memory impairment. Collectively, these findings suggested that compound **3c** was a promising artificial intelligence (AI)-driven multifunctional agent with BuChE inhibition potential for the treatment of AD.

Declaration of competing interest

The authors declare that they have no known competing financial interests or personal relationships that could have appeared to influence the work reported in this paper.

CRediT authorship contribution statement

Qiyao Zhang: Writing – original draft, Methodology, Data curation. **Yuting Li:** Validation, Data curation. **Qishun Jin:** Data curation. **Zhengwei Liu:** Data curation. **Hongsong Chen:** Data curation. **Jingqi Huang:** Data curation. **Taoyi Liu:** Data curation. **Xiaojuan Liu:** Data curation. **Zhenghuai Tan:** Supervision, Methodology, Data curation. **Shuheng Huang:** Writing – original draft, Supervision, Software, Data curation, Conceptualization. **Wu Dong:** Supervision, Investigation, Data curation. **Zhipei Sang:** Writing – review & edit-

ing, Writing – original draft, Supervision, Resources, Project administration, Investigation, Funding acquisition, Data curation, Conceptualization.

Acknowledgments

This work was financially supported by the China Postdoctoral Science Foundation (No. 2022M712153); The National Natural Science Foundation of China (Nos. 22367007 and 82304384); The Fundamental Research Funds for Hainan University (No. KYQD(ZR)23002); Hainan Provincial Natural Science Foundation of China (No. 824RC500).

Supplementary materials

Supplementary material associated with this article can be found, in the online version, at doi:10.1016/j.cclet.2025.110964.

References

[1] R. Hodson, Nature 559 (2018) S1.
[2] J.F. Zhang, Y.L. Zhang, J.X. Wang, et al., Signal Transduct. Target. Ther. 9 (2024) 211.
[3] Q. Zheng, X. Wang, Protein Cell 16 (2025) 83–120.
[4] Z.P. Sang, K.R. Wang, J.H. Dong, et al., Eur. J. Med. Chem. 238 (2022) 114464.
[5] J.B. Sun, H. Zhong, K. Wang, et al., Acta Pharm. Sin. B 11 (2021) 3417–3432.
[6] D. Knez, D. Diez-Iriepa, M. Chioua, et al., Acta Pharm. Sin. B 13 (2023) 2152–2175.
[7] E. Giacobini, A.C. Cuello, A. Fisher, Brain 145 (2022) 2250–2275.
[8] S.S. Xing, Q. Li, B.C. Xiong, et al., Med. Res. Rev. 41 (2021) 858–901.
[9] S. Darvesh, D.A. Hopkins, C. Geula, Nat. Rev. Neurosci. 4 (2003) 131–138.
[10] I. Manoharan, R. Boopathy, S. Darvesh, O. Lockridge, Clin. Chim. Acta 378 (2007) 128–135.
[11] G.A. Reid, S. Darvesh, Neuroscience 98 (2015) 424–435.
[12] T. Maurice, M. Strehaiano, N. Siméon, et al., Behav. Brain Res. 296 (2016) 351–360.
[13] L.L. Jing, W.X. Wei, B.R. Meng, et al., Bioorg. Chem. 134 (2023) 106465.
[14] J. Moreira, M. Machado, M. Dias-Teixeira, et al., Acta Pharm. Sin. B 13 (2023) 3208–3237.
[15] S.S. Panda, N. Jhanji, Curr. Med. Chem. 27 (2020) 5887–5917.
[16] K. Wojtunik-Kulesza, T. Oniszczuk, J. Mołdoch, et al., Int. J. Mol. Sci. 23 (2022) 1212.
[17] X. Chen, J. Drew, W. Berney, W. Lei, Cells 10 (2021) 1309.
[18] A.K. Desai, G.T. Grossberg, Expert Rev. Neurother. 5 (2005) 563–580.
[19] H.H. Zhang, Y.Y. Wang, Y.Q. Wang, et al., Eur. J. Med. Chem. 240 (2022) 114606.
[20] A. Matošević, A. Bosak, Arh. Hig. Rada Toksikol. 71 (2020) 285–299.
[21] M.T. Kabir, M.S. Uddin, M.M. Begum, et al., Curr. Pharm. Des. 25 (2019) 3519–3535.
[22] R. Gupta, D. Srivastava, M. Sahu, et al., Mol. Divers. 25 (2021) 1315–1360.
[23] R.Y. Choi, A.S. Coyner, J. Kalpathy-Cramer, et al., Transl. Vis. Sci. Technol. 9 (2020) 14.
[24] K. Crampon, A. Giorkallos, M. Deldossi, et al., Drug Discov. Today 27 (2022) 151–164.
[25] Z.P. Sang, P. Bai, Y.J. Ban, et al., Bioorg. Chem. 127 (2022) 106007.
[26] X.N. Wu, Y.D. Huang, J.X. Li, et al., Acta Pharm. Sin. B 8 (2018) 615–628.
[27] X.L. Deng, J. Xie, Y.Q. Li, et al., Chin. Chem. Lett. 27 (2016) 566–570.
[28] Z.P. Sang, K.R. Wang, J. Shi, et al., Eur. J. Med. Chem. 187 (2020) 111958.
[29] B. Zhen, X.Y. Suo, J. Dang, et al., Chin. Chem. Lett. 32 (2021) 2338–2341.
[30] R. Chen, X. Li, H. Chen, et al., Eur. J. Med. Chem. 251 (2023) 115253.
[31] P. Wang, Y. Wang, P. Li, et al., Chin. Chem. Lett. 34 (2023) 107691.
[32] Z.P. Sang, K.R. Wang, P.F. Zhang, et al., Eur. J. Med. Chem. 180 (2019) 238–252.
[33] E.E. Patton, L.I. Zon, D.M. Langenau, Nat. Rev. Drug Discov. 20 (2021) 611–628.
[34] H.S. Chen, J. Mi, S. Li, et al., J. Enzyme Inhib. Med. Chem. 38 (2023) 2169682.